Kinetics and thermodynamics of adsorption for arsenate ions on the hierarchical porous adsorbent of α-Fe$_2$O$_3$/Fe$_3$O$_4$/C with bamboo bio-template

Yanhong Li[a], Yinian Zhu[b],*, Zongqiang Zhu[c], Wenhui Wei[b], Huan Deng[a], Yanpeng Liang[c], Xuehong Zhang[b], Dunqiu Wang[b],*

[a]*College of Light Industry and Food Engineering, Guangxi University, Nanning 530004, China, Tel. +86 773 2536719,*
email: lyh1685@163.com (Y. Li), denghuan@glut.edu.cn (H. Deng)
[b]*College of Environmental Science and Engineering, Guilin University of Technology, Guilin 541004, China,*
Tel. +86 773 5891059, Fax +86 773 5895330, email: zhuyinian@glut.edu.cn (Y. Zhu), 345361846@qq.com (W. Wei),
zhangxuehong@x263.net (X. Zhang), wangdunqiu@sohu.com (D. Wang)
[c]*Guangxi Key Laboratory of Environmental Pollution Control Theory and Technology, Guilin University of Technology, Guilin 541004,*
China, Tel./Fax +86 773 3693255, email: zhuzongqiang@glut.edu.cn (Z. Zhu), liangyanpeng@glut.edu.cn (Y. Liang)

ABSTRACT

A novel hierarchical porous adsorbent of α-Fe$_2$O$_3$/Fe$_3$O$_4$/C (HPA-Fe/C-B) was prepared with bamboo bio-template and investigated for its adsorption capacity of arsenic(V). The result indicated that the HPA-Fe/C-B adsorbent had a specific surface area of 198.1 m^2/g and retained the hierarchical porous microstructure of bamboo with three kinds of pores (widths 50~75 μm, 1~30 μm and 0.0017~0.2891 μm) originating from vessels, fibres or parenchyma cells and pits on the walls of the vessels and parenchyma cells, respectively. With increasing initial arsenic(V) concentrations from 5 mg/L to 100 mg/L, the amounts of arsenic(V) adsorbed on the pulverized HPA-Fe/C-B adsorbent (<0.149 mm) increased from 0.50 mg/g to 4.55 mg/g at 25°C, from 0.50 mg/g to 5.33 mg/g at 35°C and from 0.50 mg/g to 4.89 mg/g at 45°C. The corresponding removal rates decreased from 99.97% to 45.58% at 25°C, from 99.98% to 53.30% at 35°C and from 100.00% to 48.94% at 45°C. At the initial arsenic(V) concentrations of 5, 10 and 50 mg/L, the adsorption capacities for the un-pulverized HPA-Fe/C-B adsorbent (>3 mm) were 0.45, 0.86 and 3.02 mg/g, respectively, which were nearly equal to the mean value for iron oxides particles or nanoparticles. The pseudo-second-order kinetic model fitted the experimental data very well. The adsorption followed both Langmuir and Freundlich isotherms.

Keywords: Bamboo bio-template; Hierarchical porous microstructure; Iron oxide adsorbent; Adsorption; Arsenate

1. Introduction

Arsenic exposure is known as a worldwide public health threat [1–3]. Arsenic, one of WHO's 10 chemicals of major public health concern, is a natural component of the earth's crust and can be released into the environment through various natural processes including volcanic emissions, microbiological activity, and weathering reactions, as well as numerous human activities, such as burning of fossil fuels and wastes, former agricultural utilization of arsenic, cement manufacturing, pharmaceutical and chemical manufacturing, mining/smelting/refining operations, pulp and paper production, and wood preservatives [1–4]. Elevated arsenic levels in natural waters and soils pose environmental health risks [5,6]. Humans are exposed to arsenic in numerous forms from a variety of sources such as drinking water and food. Long-term exposure to inorganic arsenic can cause increased human mortality, cancer in skin/lungs/urinary tracts, cardiovascular disease, diabetes and neurotoxicity [1,6]. A provisional guideline value of 0.01 mg/L for arsenic in drinking water has been recommended

*Corresponding author.

by the World Health Organization (WHO) and accepted by numerous countries [1,3,5].

Several treatment methods, such as chemical precipitation, adsorption, nanofiltration, membrane separation; reverse osmosis, solvent extraction, ion exchange, foam flotation, lime softening, biological sequestration and microbial transformation have already been developed to remove arsenic from wastewater and water [3,7]. Adsorption is the most simple and cost effective method among all the available techniques for arsenic removal [7–9]. In the last two decades, many researches have been made to examine arsenic adsorption with various adsorbents including iron oxide, activated carbon, activated alumina, aluminium hydroxide, clays, manganese green sand, rare earth oxide and fly ash [7–10]. Iron oxides such as hematite (Fe_2O_3), magnetite (Fe_3O_4), goethite (FeOOH) and granular ferric hydroxide (GFH), available in various mineralogical forms, have been found to be effective for arsenic removal owing to their low cost and tremendous adsorption affinity and the low leaching of adsorbed arsenic from exhausted adsorbent [11].

The specific surface area is an important parameter for arsenic removal [12]. Nevertheless, low surface area of iron oxides can restrict their loading capacity. Therefore, synthesis of iron oxides with high surface area can increase the loading capacity for practical application [7]. Magnetite is a very important functional material in different research areas and can effectively adsorb As(V) from water [12]. Commonly, the iron oxides with amorphous structure own a greater removal efficiency for toxic anions in comparison to those with crystalline structure. Goethite (α-FeOOH), hydrous ferric oxide (HFO) and granular ferric hydroxide are the effective adsorbents for arsenic removal from water [7,13].

Recently, nanomaterials have attracted a significant environmental attention owing to their distinctive properties, such as small size, small diffusion resistance, large surface area, large number of active sites, high reactivity, and catalytic potential facilitate more active and rapid arsenic removal than other available adsorbents [11]. However, the separation of fine nanomaterials powders of iron oxides from solution after water treatment is difficult to perform and very expensive. Furthermore, for the nanoparticles with size < 15 nm, the magnetic separation might become ineffective and the residual particles might result in some toxicological problems in the effluent. Moreover, their stability under various treatment conditions is also questionable [5,7]. Hence, developing the optimal adsorbents that can remove toxic heavy metals through fixed-bed column adsorption is an aim of numerous researchers [13].

The hierarchical porous microstructures of bioorganic plants range from the millimetre-scale (growth ring pattern of wood) to the micrometre-scale (cellulose fibre structures) [14]. Converting these microstructures into adsorbent materials can overtake these advantages and is an alternative adsorbent producing process in comparison to the conventional powder manufacturing techniques [14,15]. Great efforts were made to use pre-processed plant materials in preparing microcellular-designed ceramics, which showed the hierarchical porous microstructures like the negative duplication of the wood biotemplate [15]. The hierarchical porous adsorbents are advantageous in applications needing interconnected porosity, such as filters [16].

In this work, the bamboo wood chips were used as microstructural biotemplates for preparing the hierarchical porous adsorbent of α-Fe_2O_3/Fe_3O_4/C (HPA-Fe/C-B) by extracting with ammonia solution, impregnating with ferric solution and calcining. The adsorption of arsenic(V) was then investigated using the prepared adsorbent, which was concerned with the study of influences of initial arsenic(V) concentration, initial pH, adsorbent dose, adsorbent grain size, contact time, and temperature. The characteristic parameters of various adsorption isotherms and kinetic equations were calculated.

2. Materials and methods

2.1. Adsorbent preparation and characterization

2.1.1. Preparation

Bamboo (*Phyllostachys pubescens*) wood was collected, air-dried, and cut into rectangular chips of 30×10×3 mm³ size. Three steps, i.e., extracting with ammonia solution, impregnating with ferric solution and calcining, were adopted in the manufacturing process of the hierarchical porous adsorbent of α-Fe_2O_3/Fe_3O_4/C (HPA-Fe/C-B) from bamboo bio-template.

In order to effectively improve the cellular and pore connectivity, the chips of bamboo wood (30×10×3 mm³) were boiled in 5% dilute ammonia solution for 6 h to remove the bamboo extractive components including fats, fatty acid, tropolones and gums, etc. The pre-treated biotemplates of bamboo wood were then cleaned with pure water and dried at 80°C for 24 h.

A 1.2 mol/L precursor solution was prepared by dissolving ferric nitrate ((Fe(NO$_3$)$_3$·9H$_2$O, analytically pure) in an ethanol-water mixture solvent (1:1), and the pre-treated bamboo biotemplates were then dipped in the ferric nitrate precursor solution at 60°C in covered glass containers. To keep the wood biotemplates always immersed in the precursor solution, it is needed to add some ferric nitrate solution in this process. The biotemplates were taken out after soaking for 3 d, and then dried in an electric furnace at 80°C for 1 d. The above soaking–drying process was repeated three times.

Finally, the dried bamboo biotemplates were putted in a stainless steel retort and carbonized in a muffle furnace at the temperature of 600°C for 3 h. The biotemplates were then cooled to room temperature so that the hierarchical porous adsorbent of α-Fe_2O_3/Fe_3O_4/C (HPA-Fe/C-B) was prepared.

2.1.2. Characterization

The chemical component of the hierarchical porous adsorbent of α-Fe_2O_3/Fe_3O_4/C (HPA-Fe/C-B) was analysed by Element Analyzer (EA2400II, PerkinElmer). The specific surface area of the HPA-Fe/C-B adsorbent was calculated from N$_2$ adsorption/desorption isotherms determined at –194°C (boiling point of N$_2$ at atmospheric pressure) using a Quantachrome NOVAe1000. For the pH$_{PZC}$ determination of the HPA-Fe/C-B adsorbent, the pHs of the suspensions containing 10 mg solid in 50 mL ultrapure water were adjusted to 1, 2, 3, 4, 5, 6, 7, 8 and 9 using HNO$_3$ and NaOH solutions.

The zeta potentials were then recorded by microelectrophoresis using a zeta potential analyzer (Zetasizer Nano ZS90, Malvern). The pH_{PZC} was determined by interpolating the data to zero zeta potential. All prepared solids before and after As(V) adsorption were characterized by powder X-ray diffraction (XRD) with a diffractometer (X'Pert PRO, PANalytical B.V.) using Cu Kα radiation (40 kV and 40 mA). Phases of the prepared materials were identified by comparing their XRD patterns with the reference code 00-005-0637 for hematite (α-Fe_2O_3), the reference code 01-089-0688 for magnetite (Fe_3O_4) and the reference code 00-001-0646 for carbon (graphite) from the ICDD standards. The morphology was observed using scanning electron microscopy (Jeol JSM-6380LV, Japan Electron Optics Ltd.). Meanwhile, the chemical composition was also analysed by the means of energy dispersive x-ray spectroscopy (EDS). Additionally, the adsorbent was characterised over the range of 4000~400 cm⁻¹ using a FT-IR spectrophotometer (Nicolet Nexus 470, Thermo Fisher Scientific Inc.) in a form of KBr pellets.

2.2. Adsorption experiments

Arsenic(V) solutions were prepared from sodium arsenate ($Na_3AsO_4 \cdot 12H_2O$, analytically pure), nitric acid (HNO_3) and ultrapure water. The batch adsorption experiments were made in a series of 100 mL plastic centrifuge tubes by agitating a certain amount of the pulverized or un-pulverized HPA-Fe/C-B adsorbent in 50 mL As(V) solutions of certain concentration and pH with an isothermal shaker (25°C) at the speed of 150 rpm for 72 h to approach chemical equilibrium between the adsorbent and the arsenic solution. All samples were centrifuged at 4000 rpm for 5 min and filtered through 0.22 μm micropore membranes, and then the residual arsenic concentrations were measured.

Various As(V) concentrations (5, 10 and 50 mg/L) were used to investigate the influence of contact time on adsorption at 25°C. Influence of adsorbent particle size was examined with different adsorbent grain sizes [un-pulverized chip (>3 mm), 20~40 mesh (0.841~0.4 mm), 40~60 mesh (0.4~0.25 mm), 60~80 mesh (0.25~0.177 mm), 80~100 mesh (0.177~0.149 mm), <100 mesh (<0.149 mm)] and 50 mL of 50 mg/L arsenic solutions at 25°C. As comparison, the carbonized bamboo (bamboo charcoal), the bamboo sawdust and α-Fe_2O_3 were also tested in the adsorption experiment to investigate the influence of the hierarchical porous structure on the adsorption capacity. Influence of pH was examined by agitating the solutions of various pHs (1, 2, 3, 4, 5, 6, 7, 8, 9, 10, 11 and 12) with 0.5 g/50 mL adsorbent dose for 5, 10 and 50 mg/L As(V) concentrations at 25°C. Nine initial As(V) concentrations (5, 10, 15, 20, 30, 40, 50, 75 and 100 mg/L) were used to investigate the influence of initial concentrations on adsorption at the initial pH 3 and the temperatures of 25, 35 and 45°C. Influence of adsorbent dose was researched with various adsorbent amounts (0.1, 0.2, 0.3, 0.4, 0.5, 0.6, 0.7, 0.8, 0.9 and 1.0 g) in 50 mL of 5, 10 and 50 mg/L As(V) solutions at the initial pH 3 and the temperature of 25°C. Kinetic experiment was made by agitating 0.5 g of the HPA-Fe/C-B adsorbent in 50 mL of 5, 10 and 50 mg/L As(V) solutions at the initial pH 3 and the temperatures of 25, 35 and 45°C in 100 mL centrifuge tubes with an agitation speed of 200 rpm. The aqueous sampling was carried out from different centrifuge tubes at the time intervals

of 5, 10, 15, 20, 30, 60, 120, 180, 240, 300, 360, 420, 480, 540, 720, 1080 and 1440 min. Adsorption isotherms were determined by agitating 0.5 g of the HPA-Fe/C-B adsorbent in 50 mL of As(V) solutions of different concentrations (5, 10, 15, 20, 30, 40, 50, 75 and 100 mg/L) at the initial pH 3 and the constant temperatures of 25°C, 35°C and 45°C in 100 mL centrifuge tubes at the speed of 200 rpm for 6 h to approach chemical equilibrium between the adsorbent and the As(V) solutions.

The residual aqueous As(V) concentrations were analysed using AAS (flame & graphite furnace atomic adsorption spectrophotometer, AA 700, Perkin-Elmer) under the operating conditions after the instrument manual. The As(V) removal rates (R) are calculated as follows: R (%) = ($C_o - C_e$)/$C_o \times 100$, where C_o and C_e are the initial and the equilibrium As(V) concentrations, respectively. The adsorption amount at the time t, q_t (mg/g), is calculated according to: $q_t = (C_o - C_t)V/W$, where C_t (mg/L) is the aqueous As(V) concentration at the time t. V and W are the volume of the solution (L) and the mass of the adsorbent used (g), respectively.

3. Results and discussion

3.1. Characterization of the adsorbent

The C, H, O, N and S contents of the hierarchical porous adsorbent of α-Fe_2O_3/Fe_3O_4/C (HPA-Fe/C-B) prepared with bamboo bio-template were measured to be 25.18~25.85%, 1.02~1.49%, 25.61~26.08%, 0.85~0.99% and 0.18~0.24%, respectively. The total Fe content of the HPA-Fe/C-B adsorbent was determined to be 45.51~47.02%.

The specific surface area of the HPA-Fe/C-B adsorbent was estimated to be 198.1 m²/g through the Brunauer-Emmett-Teller (BET) method using N_2 adsorption isotherm at 77 K. The HPA-Fe/C-B adsorbent demonstrated a type IV N_2 adsorption isotherm, according to Brunauer-Deming-Deming-Teller (BDDT) classification. Two capillary condensation steps indicated bimodal pore-size distributions in the mesoporous and microporous regions [17]. The magnitude of the specific surface area of the un-pulverized HPA-Fe/C-B adsorbent is comparable to the BET surface areas of synthetic and natural iron oxides [10,18–20]. The pH_{PZC} values of the HPA-Fe/C-B adsorbent, Fe_3O_4, α-Fe_2O_3 and the bamboo charcoal were 3.1, 5.7, 5.2 and 2.3, respectively.

The XRD characterization of the HPA-Fe/C-B adsorbent before and after As(V) adsorption indicated that the HPA-Fe/C-B adsorbent consisted of hematite (α-Fe_2O_3), magnetite (Fe_3O_4) and carbon (Fig. 1). The recorded XRD patterns agreed well with the hematite and magnetite references in both peak position and relative intensity. The recorded diffraction peaks at 2θ = 24.11°, 33.13°, 35.61°, 40.85°, 49.44°, 54.04°, 57.50°, 62.42° and 63.98° corresponded to the (012), (104), (110), (113), (024), (116), (122), (214) and (300) reflection peaks of the standard reference code 00-005-0637 for hematite (α-Fe_2O_3) [21,22]. The diffraction peaks at 2θ= 30.22°, 35.61°, 43.34°, 57.50° and 62.42° were identified as the (220), (311), (440), (511) and (440) reflection peaks of the standard reference code 01-089-0688 for magnetite (Fe_3O_4) [21,23]. The diffraction peaks at 42.81° and 44.62° were in agreement with the reference code 00-001-0646 for carbon (graphite). A quantitative analysis of the XRD profile using the Rietveld method indicated that the iron oxides of the
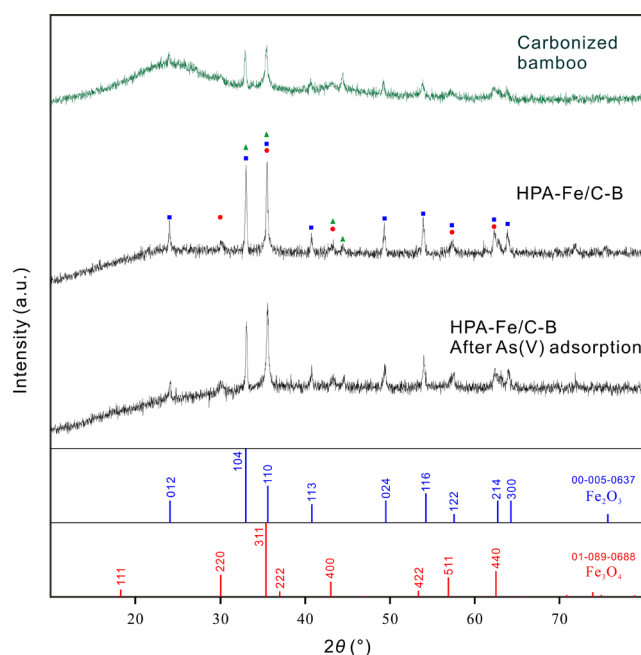
Fig. 1. XRD patterns of the HPA-Fe/C-B adsorbent prepared with bamboo bio-template (A) before and (B) after the As(V) adsorption.

Fig. 2. FT-IR analysis result of the HPA-Fe/C-B adsorbent prepared with bamboo bio-template (A) before and (B) after the As(V) adsorption.

HPA-Fe/C-B adsorbent consisted of 59.78 wt-% of magnetite and 40.22 wt-% of hematite. As showed in Fig. 1, the composition and properties of the HPA-Fe/C-B adsorbent before and after As(V) adsorption were indistinguishable.

The FT-IR spectra of the HPA-Fe/C-B material are shown in Fig. 2. Infrared analysis of the HPA-Fe/C-B adsorbent showed OH stretching at 3423.09 cm^{-1}, hydroxyl bending and γ'(OH) water bending vibration or overtones of hydroxyl bending around 1613.62 cm^{-1}. The Fe–O vibration band was seen at 469.47 cm^{-1}. The band at around 1380.70 cm^{-1} was attributed to an Fe–O stretching vibration. Moreover, the Fe–OH bending vibration was observed at around 1022.10 cm^{-1}. In the FT-IR spectra of the HPA-Fe/C-B adsorbent after adsorption of As(V), the peaks of AsO_4^{3-} for the As-O stretching appeared around 829.06~890.35 cm^{-1} (Fig. 2).

The HPA-Fe/C-B adsorbent retained the hierarchical porous microstructure of bamboo with three kinds of pores: (1) macropores (widths 50~75 μm) originating from vessels; (2) mesopores (widths 10~30 μm) originating from parenchyma cells and mesopores (widths 1~15 μm) originating from fibres; and (3) micropores (widths 0.0017~0.2891 μm) formed on the walls of the vessels and parenchyma cells giving pits (Fig. 3). The SEM observation also showed that the extracting pre-treatment could remove the bamboo extractive components including tylosises, fats, fatty acid, tropolones and gums and obviously increase the connectivity among different pores (Fig. 3). Quantitative SEM-EDS analysis indicated that the As(V) adsorbed on the HPA-Fe/C-B adsorbent was up to 4.27% (w:w) (Fig. 4). The EDS spectra were recorded on the adsorbents treated with a higher As(V) concentration (100 mg/L) other than that in the batch equilibrium and kinetic experiments. The characteristic arsenate peaks at 1.42 keV in the EDS spectrum confirmed the binding of arsenate onto the HPA-Fe/C-B surface.
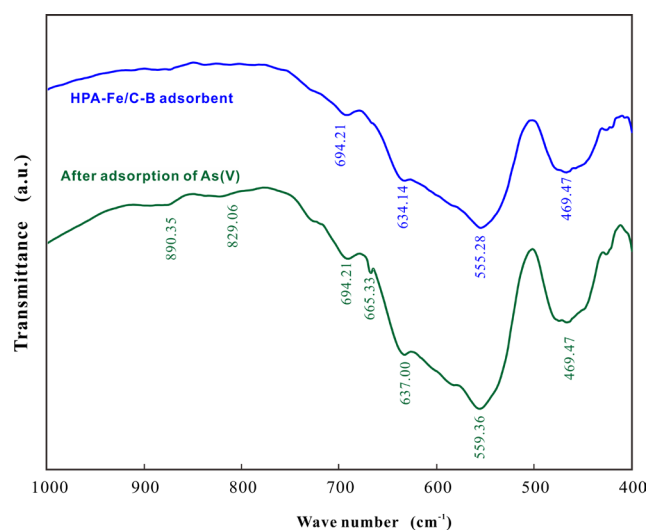
3.2. Influences of adsorption conditions

Adsorption equilibrium can be dominated by many adsorption factors, e.g., the properties of solute and adsorbent as well as the solution pH. In this work, the influences of the contact time, the initial As(V) concentration, temperature, solution pH, adsorbent mass and particle size on adsorption kinetics were to be examined.

3.2.1. Influence of contact time

The residual aqueous As(V) concentrations decreased quickly with the contact time, which indicated a strong interaction between the As(V) ions and the adsorbent (Fig. 5). The amount of As(V) adsorbed (mg/g) increased with time until it slowly reached equilibrium owing to a constant decreasing in the driving force ($q_e - q_t$). The amount of As(V) adsorbed and the residual As(V) concentrations in solutions were nearly steady after adsorption for 20, 360 and 720 min at initial pH 3 and 25°C with the initial As(V) concentrations of 5, 10 and 50 mg/L, respectively. This pseudo-equilibrium time of 20~720 min was shorter than 24 h for the As(V) adsorption on natural hematite (0.25~0.50 mm) [24].

For the adsorption with the initial As(V) concentration of 5 mg/L at pH 3 and 25°C, most of As(V) was adsorbed in the early 20 min at a mean adsorption rate of 0.0248 mg/(g·min) (99.25% of total amount of As(V) adsorbed). Similar trends were also found for the adsorption with the initial As(V) concentrations of 10 and 50 mg/L in the early 180 and 720 min, respectively. The reaction time play a significant role in adsorption. For the physical adsorption, most of the sorbate species can be adsorbed in a short time. Conversely, the strong chemical binding between sorbate and adsorbent needs a longer reaction time to attain equilibrium. Previous adsorption researches also indicated that the uptake of sorbate species was faster at the initial stage of adsorption, and then it became slower near equilibrium. Large numbers of vacant sites available on the adsorbent surface may result in the initial rapid uptake of adsorbate species [25].
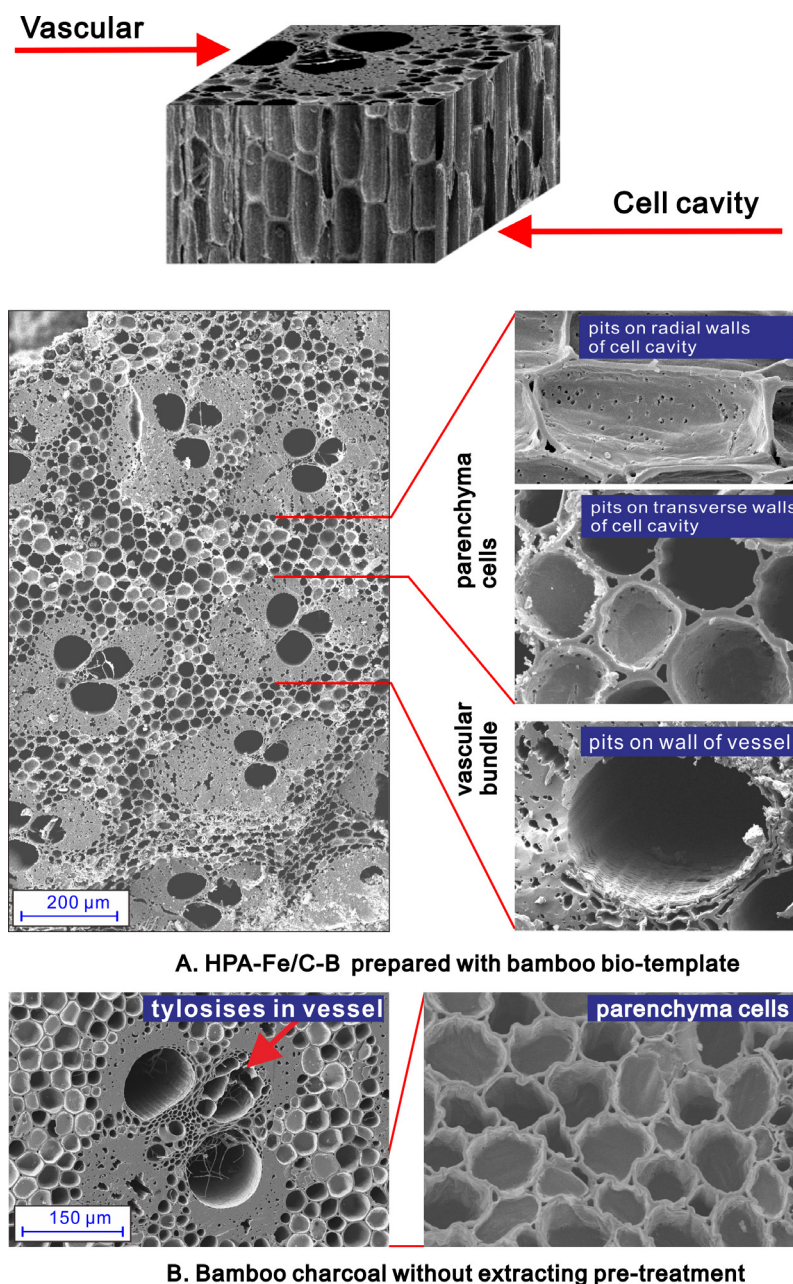
Fig. 3. SEM result of the HPA-Fe/C-B adsorbent prepared with bamboo bio-template and the bamboo charcoal without extracting pre-treatment.

3.2.2. Influence of initial concentration and temperature

The kinetic dependencies on initial concentration and temperature were also examined by varying initial As(V) concentrations (5~100 mg/L) and temperatures (25, 35 and 45°C), while the other adsorption conditions were kept constant (initial pH 3, adsorbent dose 0.5 g/50 mL). The amount of As(V) adsorbed (q_e) and the removal rate versus the initial concentrations are illustrated in Fig. 6. The overall trends for the adsorption at different temperatures were similar. With the increasing initial As(V) concentrations from 5 mg/L to 100 mg/L, the amount of As(V) adsorbed increased from 0.50 mg/g to 4.55 mg/g at 25°C, from 0.50 mg/g to 5.33 mg/g at 35°C, and from 0.50 mg/g to 4.89 mg/g at 45°C. Correspondingly, the adsorption removal rates decreased constantly from 99.97% to 45.58% at 25°C, from 99.98% to 53.30% at 35°C, and from 100.00% to 48.94% at 45°C.

3.2.3. Influence of initial solution pH

Not only the surface charge of the adsorbent, but also the solution As(V) chemistry could be significantly influenced by the solution pH (Fig. 7). Because the specific adsorption mechanism was dominant, increasing pH results in the decreasing in the surface $FeOH_2^+$ groups [8].
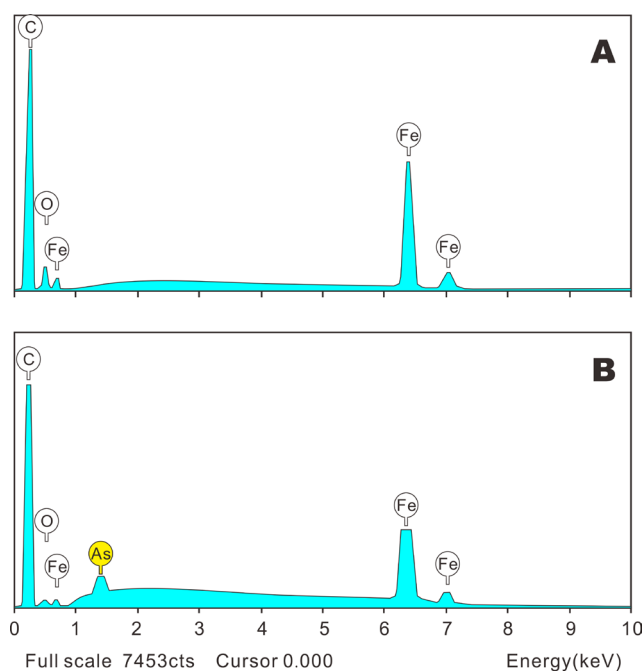
Fig. 4. SEM-EDS analysis result of the HPA-Fe/C-B adsorbent prepared with bamboo bio-template (A) before and (B) after the As(V) adsorption.
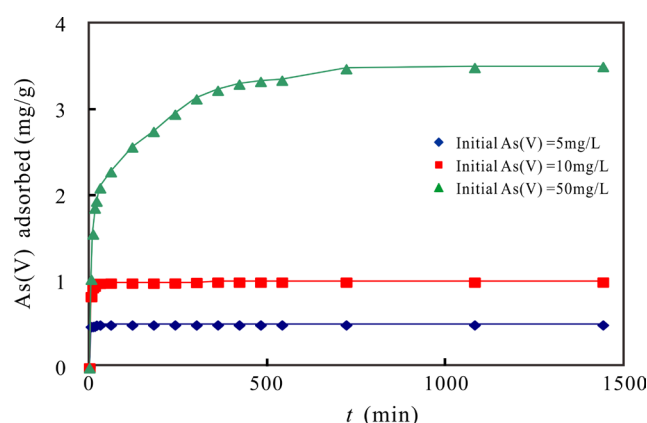
Fig. 5. Influence of contact time on the As(V) adsorption onto the HPA-Fe/C-B adsorbent (initial pH 3; adsorbent dose 0.5 g/50 mL; 25°C).

As(V) existed as arsenate anions in aqueous solution. The adsorption of the negative charged arsenate anion groups onto the adsorbent surface was mainly affected by the surface charge of the adsorbent, which was dominated by solution pH [26]. Low initial pH benefited the As(V) adsorption onto the HPA-Fe/C-B adsorbent. For the initial As(V) concentrations of 5 and 10 mg/L with pH 3, most of the arsenate anions could be adsorbed from aqueous solution, and the removal rates reached 99.95%~99.98% and decreased to 72.41%~88.06% with the pH increasing from 3 to 10. For the initial As(V) concentrations of 50 mg/L, the adsorption capacity decreased from 3.28 mg/g to 2.13 mg/g and the removal rate decreased from 65.66% to 42.60% with the pH increasing from 3 to 10.
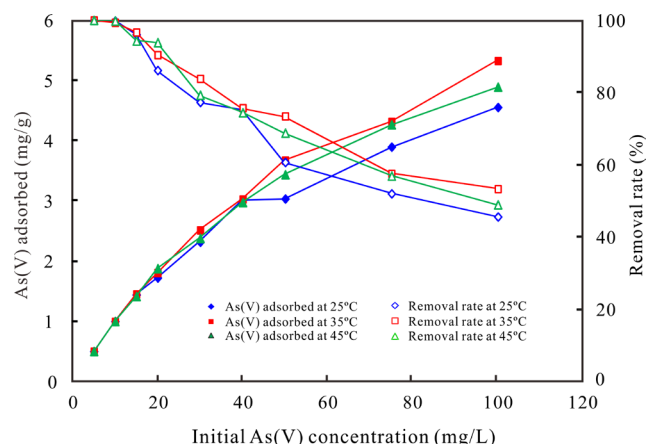
Fig. 6. Influence of initial concentration and temperature on the As(V) adsorption onto the HPA-Fe/C-B adsorbent (initial pH 3; adsorbent dose 0.5 g/50 mL; adsorbent grain size <100 mesh).
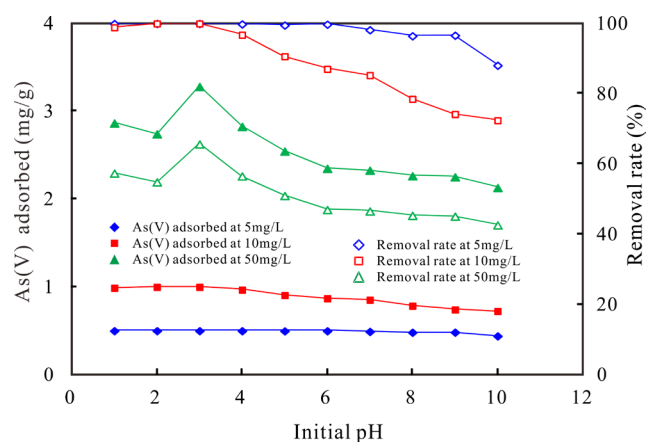
Fig. 7. Influence of initial pH on the As(V) adsorption onto the HPA-Fe/C-B adsorbent (initial concentration 5, 10 and 50 mg/L, adsorbent dose 0.5 g/50 mL; adsorbent grain size < 100 mesh; 25°C).

3.2.4. Influence of adsorbent dose

The total As(V) amount adsorbed increased with the increasing adsorbent dose of HPA-Fe/C-B (Fig. 8), which was considered to be related to increased adsorbent surface area and availability of more adsorption sites. On the other hand, the unit adsorption capacity decreased with the increasing adsorbent dose, which was related to the possible aggregation or overlapping of adsorbent surface area accessible to arsenate ions and the increasing of diffusion path length. For the initial As(V) concentrations of 5, 10 and 50 mg/L, the amounts of As(V) adsorbed decreased from 2.19 mg/g to 0.25 mg/g, 4.62 mg/g to 0.50 mg/g and 8.31 mg/g to 2.09 mg/g with the increasing adsorbent mass from 0.1 to 1.0 g in 50 mL solution, respectively. The corresponding removal rates for As(V) increased constantly from 89.92% to 99.99%, 92.94% to 99.99% and 33.27% to 83.52%.
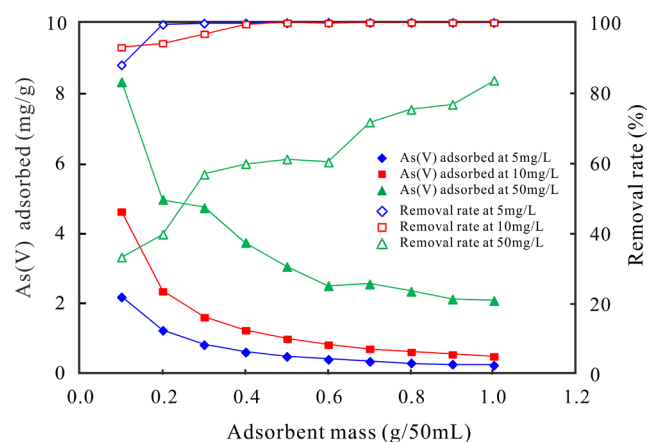
Fig. 8. Influence of adsorbent dose on the As(V) adsorption onto the HPA-Fe/C-B adsorbent (initial pH 3; initial concentration 5, 10 and 50 mg/L; adsorbent dose 0.5 g/50 mL; adsorbent grain size <100 mesh; 25°C).

3.2.5. Influence of adsorbent grain size

The adsorption capacities were determined for the adsorption at different initial As(V) concentrations (5, 10 and 50 mg/L) at 25°C, while other adsorption condition was kept constant. The dependency of the amount of As(V) adsorbed (q_e) and the removal rate on the initial As(V) concentration is plotted in Fig. 9. The amounts of As(V) adsorbed on the un-pulverized HPA-Fe/C-B adsorbent (>3 mm) were 0.45, 0.86 and 3.02 mg/g for the adsorption at the initial As(V) concentrations of 5, 10 and 50 mg/L, respectively, and the corresponding removal rates were 90.75%, 86.66% and 61.24%. This means that the un-pulverized HPA-Fe/C-B adsorbent possessed a greater adsorption capacity and a greater adsorption removal rate than the bamboo charcoal and the bamboo sawdust at various initial As(V) concentrations. At the initial As(V) concentrations of 5, 10 mg/L 50 mg/L, the un-pulverized HPA-Fe/C-B adsorbent had a higher adsorption capacity and a higher removal efficiency than the Fe_2O_3 powder.

Fig. 9 also indicates that the As(V) adsorption capacities and removal rates were dependent on the particle sizes of the pulverized HPA-Fe/C-B adsorbents and the initial As(V) concentrations. The adsorption capacities increased and the adsorption rates decreased with the increasing initial As(V) concentrations for all pulverized HPA-Fe/C-B adsorbents. But for the adsorption at low initial As(V) concentrations, the influences of the initial As(V) concentrations and the particle sizes of the pulverized HPA-Fe/C-B adsorbents on the adsorption removal rates were insignificant. For the adsorption of As(V) on the pulverized HPA-Fe/C-B adsorbents at the initial As(V) concentrations of 5, 10 and 50 mg/L, the minimum adsorption capacity and removal efficiency of arsenic were observed for the pulverized HPA-Fe/C-B sample of 60~40 mesh (0.25~0.4 mm) to be 0.23~1.41 mg/g and 28.30%~46.54%, respectively. The highest As(V) adsorption capacity and removal rate were determined for the pulverized HPA-Fe/C-B adsorbent of <0.149 mm (<100 mesh) to be 0.50~3.16 mg/g and 63.21~99.91%, respectively. Comparatively, the un-pulverized HPA-Fe/C-B adsorbent (chip, >3 mm) also had a high adsorption capacity
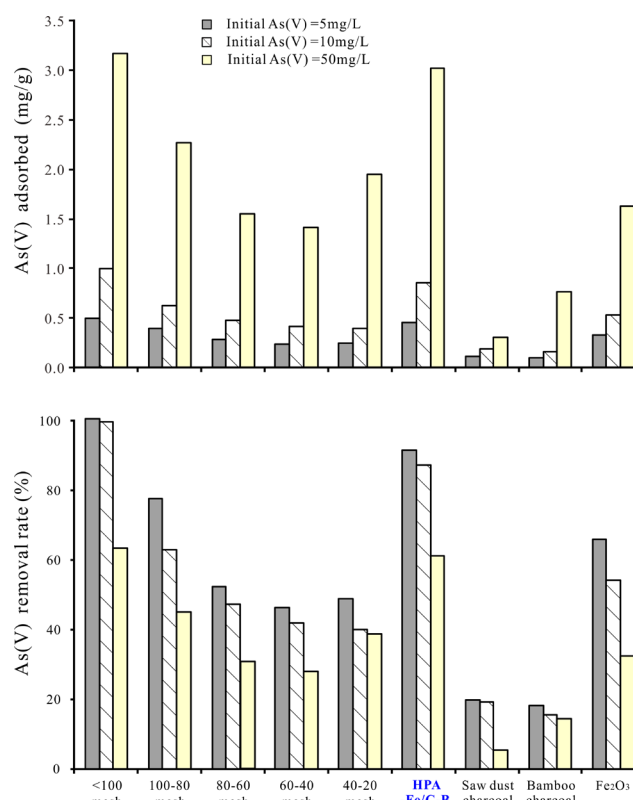
Fig. 9. Adsorption of As(V) by the HPA-Fe/C-B adsorbent (different grain sizes), the bamboo charcoal, the charcoal from bamboo saw dust and the Fe_2O_3 powder (initial pH = 3; initial concentration 5, 10 and 50 mg/L; adsorbent dose 0.5 g/50 mL; 25°C).

(0.45~3.02 mg/g) and removal rate (61.24%~90.75%) for the adsorption at the initial As(V) concentration of 5~50 mg/L, owing to the hierarchical porous microstructure of the HPA-Fe/C-B adsorbent prepared with bamboo bio-template.

3.3. Comparison of max adsorption capacity of As(V) by iron oxides adsorbents

Table 1 presents a comparison of the HPA-Fe/C-B adsorbent with some iron oxides and iron-oxide-coated adsorbents for the arsenate adsorption removal from water in literatures [10,12,27–34].

The adsorption capacity of As(V) of the un-pulverized HPA-Fe/C-B adsorbent (chip, >3 mm) was higher than those of natural and synthetic iron oxide based adsorbents. The As(V) adsorption onto natural hematite, magnetite and goethite was examined comprehensively [29]. The As(V) adsorption capacities were determined to be 0.10 mg/g for natural hematite (particle size 0.25 mm, specific surface area 0.38 m^2/g), 0.12 mg/g for natural magnetite (particle size 0.10 mm, specific surface area 0.89 m^2/g) and 0.20 mg/g for natural goethite (particle size 0.25 mm, specific surface area 2.01 m^2/g) [29]. Additionally, the maximum As(V) adsorption capacities were measured to be 0.85, 0.41 and 1.22 mg/g for three commercial mineral adsorbents, i.e., magnetite (specific surface area 1.6 m^2/g), hematite (particle size 0.05 mm, specific surface area 1.66 m^2/g) and goethite (particle

Table 1
Comparison of adsorption capacity of the HPA-Fe/C-B adsorbent with some iron oxides for As(V) removal

Adsorbent	pH	Concentr. (mg/L)	Surface area (m²/g)	Grain size (mm)	T (°C)	Capacity (mg/g)	Ref.
HPA-Fe/C-B	3	5	198.1	>3	25	0.45	This study
HPA-Fe/C-B	3	10	198.1	>3	25	0.86	This study
HPA-Fe/C-B	3	50	198.1	>3	25	3.02	This study
HPA-Fe/C-B	3	5–100	–	<0.149	25	4.50	This study
HPA-Fe/C-B	3	5–100	–	<0.149	35	5.23	This study
HPA-Fe/C-B	3	5–100	–	<0.149	45	4.90	This study
α-Fe$_2$O$_3$	3	5	–	<0.25	25	0.33	This study
α-Fe$_2$O$_3$	3	10	–	<0.25	25	0.54	This study
α-Fe$_2$O$_3$	3	50	–	<0.25	25	1.63	This study
Magnetite	6.5	0.075–75	0.89	0.1	room	0.12	[29]
Magnetite	6	0.075–15	1.6	–	room	0.85	[31]
Magnetite	4	0.5	–	28 nm	–	1.58	[30]
Magnetite	6	0.3–100	–	17 nm	–	4.78	[33]
Magnetite	4.8–6.1	0–33.71	3.7	300 nm	room	0.75–1.08	[10]
Magnetite	4.8–8	0–33.71	60	20 nm	room	5.95–11.41	[10]
Magnetite 98%, minor Hematite	5	5	6.58	–	–	0.05	[32]
Hematite	7.3	0.075–75	0.38	0.25	room	0.10	[29]
Hematite	6	0.075–15	1.66	0.05	room	0.41	[31]
Hematite	6	0.3–100	–	12 nm	–	4.90	[33]
Hematite 96%–98%, minor Quartz	5	5	3.77	–	–	0.21	[32]
Hematite 80.8%	4.2	10	14.4	0.200	30	0.20	[27]
Goethite	7.5	0.075–75	2.01	0.25	room	0.20	[29]
Goethite	6	0.075–15	11.61	0.01	room	1.218	[31]
Goethite 99%	5	5	12.1	–	–	0.05	[32]
Iron oxide pillared clays	6	0.2–2	275	–	28	0.026	[7]
Iron-impregnated biochar	5.8	0.1–55	16	–	20	2.16	[35]
Fe-hydrotalcite supported magnetite nanoparticle	9	0.1~2	–	50 nm	–	1.28	[36]
ACs modified with Fe hydro(oxide) nanoparticles	6–8	0.025–1.5	1045	3–36 nm	–	0.37–1.25	[37]

size 1.22 mm, specific surface area 11.61 m²/g), respectively [31]. The Langmuir isotherm model fitted well the arsenate adsorption data for all adsorbents, indicating a monolayer adsorption of arsenate onto the iron oxide adsorbents [31]. The As(V) adsorption capacities of the un-pulverized HPA-Fe/C-B adsorbent at the initial As(V) concentrations of 5, 10 and 50 mg/L were 0.32, 0.63 and 1.58 times 1.575 mg/g, respectively, which was reported to be the As(V) adsorption capacity for the synthetic magnetite nano-adsorbent (particle size of 28 nm) [30].

These natural iron oxide minerals showed similar adsorption capacities for arsenate to synthetic iron oxide based adsorbents. The difference in the adsorption capacities of natural and synthetic magnetite adsorbents might result from the difference in their specific surface areas. The BET surface areas of the 300 and 20 nm magnetites were 3.7 m²/g and 60 m²/g, respectively [10]. The As(V) adsorption capacity of the commercially obtainable 20-nm magnetite (5.95~11.41 mg/g) was nearly 8~10 times that of the commercially obtainable 300-nm magnetite (0.75~1.08 mg/g) [10].

The smaller sizes of magnetite (Fe$_3$O$_4$) nano-adsorbents were favourable for the diffusion of arsenate anions from water to the active sites on the adsorbents. Nevertheless, nano-materials tend to aggregate in water, which might limit their adsorption effectiveness. In general, in order to enhance mobility and reactivity, nano-materials should be stable in water to avoid aggregation and sedimentation, which may limit the large-scale application [34]. Although the removal rate was the highest with the smallest particle size, it is not suitable for column application, due to potential clogging and serious hydraulic obstruction when waste streams flow through columns [24].

Additionally, the un-pulverized HPA-Fe/C-B adsorbent exhibited also a higher arsenate adsorption capacity than iron-oxide-coated adsorbents in the literatures, such as iron oxide pillared clays [7], iron-impregnated biochar [35], Fe-hydrotalcite supported magnetite nanoparticle [36] and activated carbons modified with iron hydro (oxide) nanoparticles [37]. A decreasing of the specific surface areas from 256 m^2/g for biochar to 16.0 m^2/g for Fe-impregnated biochar suggested that Fe-impregnation could clog pore-openings or fill pores on biochar surfaces [35]. The soaking–drying process of the present work has overcome this disadvantage.

3.4. Adsorption kinetics

3.4.1. Pseudo-first-order kinetic model

The pseudo-first-order kinetic model is expressed by the following equation [38]:

$$\ln(q_e - q_t) = \ln q_e - k_1 t \tag{1}$$

where q_e is the equilibrium adsorption capacity (mg/g), q_t the amount of As(V) adsorbed (mg/g) at time t (min), and k_1 the rate constant of the pseudo-first-order kinetics (min^{-1}).

Plotting of $\ln(q_e - q_t)$ versus t yields a straight line with intercept $\ln q_e$ and slope $-k_1$ (Fig. 10). The k_1 and q_e values for the As(V) adsorption onto the HPA-Fe/C-B adsorbent are listed in Table 2. As showed in Table 2, the correlation coefficients (R^2) were 0.5798, 0.8285 and 0.9243 for the adsorption at the initial As(V) concentrations of 5, 10 and 50 mg/L, respectively. This means that the pseudo-first-order kinetic model did not fit well to the experimental data.

3.4.2. Pseudo-second order kinetic model

The pseudo-second-order kinetic model is described as following [39]:

$$\frac{t}{q_t} = \frac{1}{k_2 q_e^2} + \frac{t}{q_e} \tag{2}$$

where k_2 is the pseudo-second-order constant (g/(mg·min)). The initial adsorption rate (h) (mg/(g min)) can be calculated using the following equation:

$$h = k_2 q_e^2 \tag{3}$$
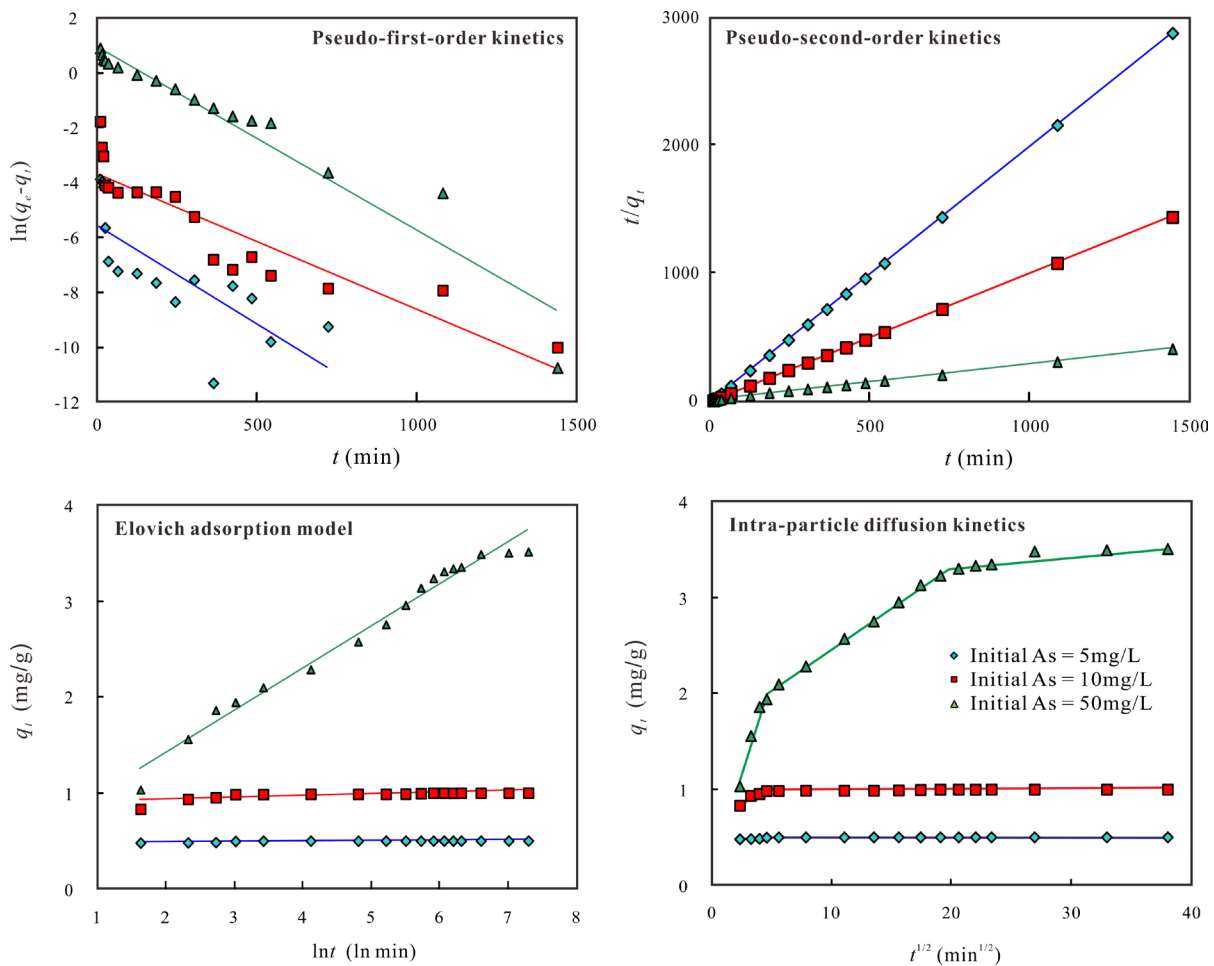
Fig. 10. Kinetics for the As(V) adsorption onto the HPA-Fe/C-B adsorbent (initial pH 3; adsorbent dose 0.5 g/50 mL; adsorbent grain size <100 mesh; 25°C).

Table 2
Kinetic and isotherm parameters for the As(V) adsorption onto the HPA–Fe/C-B adsorbent

Pseudo-first-order constants			
Initial As(V) concentration (mg/L)	k_1 (1/min)	q_e (mg/g)	R^2
5	0.0072	0.0036	0.5798
10	0.0049	0.0245	0.8285
50	0.0067	0.3852	0.9243

Pseudo-second-order constants				
Initial As(V) concentration (mg/L)	k_2 (g/(mg·min))	h (g/(mg·min))	q_e (mg/g)	R^2
5	8.3819	2.0938	0.4998	1.0000
10	0.9086	0.9079	0.9996	1.0000
50	0.0093	0.1188	3.5714	0.9989

Elovich *constants*			
Initial As(V) concentration (mg/L)	a_e (mg/g·min)	b_e (g/mg)	R^2
5	4.60E+62	312.50	0.6453
10	3.65E+19	55.25	0.5674
50	1.51E+00	2.28	0.9798

Intra-particle diffusion constants (Fitting data with single straight line)		
Initial As(V) concentration (mg/L)	K_d (mg/(g·min$^{1/2}$))	R^2
5	0.0004	0.3796
10	0.0022	0.3304
50	0.0649	0.8134

Langmuir constants				
Temperature (°C)	q_m (mg/g)	K_L (L/mg)	R_L	R^2
25	4.50	0.2856	0.0338–0.4119	0.9675
35	5.23	0.3091	0.0313–0.3928	0.9660
45	4.90	0.3103	0.0312–0.3920	0.9728

Freundlich constants			
Temperature (°C)	K_F (mg$^{1-1/n}$L$^{1/n}$g^{-1})	$1/n$	R^2
25	1.7771	0.1949	0.9615
35	1.9203	0.2153	0.9682
45	2.0101	0.1711	0.9456

The pseudo-second-order constants (k_2) and the equilibrium adsorption capacity (q_e) can be determined from the intercept and slope of a straight line of plotting t/q_t versus t (Fig. 10).

The correlation coefficients ($R^2 = 0.9989\sim1.0000$) were closer to unity; therefore, the As(V) adsorption onto the the HPA-Fe/C-B adsorbent could very well be fitted by the pseudo-second-order kinetic model, suggesting that the rate-limiting step is chemi-adsorption. The k_2 and h values were 0.0093~8.3819 g/(mg·min) and 0.1188~2.0938 mg/(g·min), respectively (Table 2). The calculated equilibrium adsorption capacity (q_e) was equal to the actual value.

3.4.3. Elovich adsorption model

The linear form of the Elovich adsorption equation is expressed as follows [40]:

$$q_t = \frac{\ln a_e b_e}{b_e} + \frac{1}{b_e} \ln t \tag{4}$$

where a_e and b_e are the initial adsorption rate (mg/g min) and the constant about surface coverage and activation energy (g/mg), respectively.

Plotting of q_t versus $\ln t$ is illustrated in Fig. 10. The a_e and b_e parameters for the adsorption at various initial As(V) concentrations are calculated and listed in Table 2. The correlation coefficients ($R^2 = 0.6453\sim0.9798$) indicated that the As(V) adsorption on the HPA-Fe/C-B adsorbent did not well follow the Elovich adsorption kinetics.

3.4.4. Intra-particle diffusion kinetic model

The equation to describe The intra-particle diffusion kinetic model is given as [41]:

$$q_t = K_d t^{1/2} + C \tag{5}$$

where K_d is the rate constant of the intra-particle diffusion kinetic model (mg/(g min$^{1/2}$)). The constant C is positively correlated with the boundary layer thickness of adsorption.

In Fig. 10 plot of q_t vs. $t^{1/2}$ is presented for As(V) adsorption of the HPA-Fe/C-B adsorbent. The linear plots indicated the great pore diffusion and the instantaneous utilization of the available adsorbing sites on the HPA-Fe/C-B surface. The K_d values calculated from the straight line slopes were 0.0004~0.0649 g/(mg·min$^{1/2}$). As showed in Table 2, the correlation coefficients (R^2) for As(V) adsorption on the HPA-Fe/C-B adsorbent varied within 0.3304~0.8134. The low R^2 values did not indicate that the intra-particle diffusion was not the adsorption rate-controlling step [42]. In fact, the plot of q_t versus $t^{1/2}$ for the intra-particle transport showed a multi-linearity (Fig. 10). The adsorption of arsenate on the HPA-Fe/C-B adsorbent surface may proceed in three steps: (1) migration of arsenate to the surface due to diffusion potential and mass transfer across the external boundary layer of solution surrounding the particles, (2) dissociation (or deprotonation) of complexed aqueous arsenate, and (3) surface complexation [11,43]. Generally, the rate-controlling mechanism can be one or any combination of these three steps [25,26].

3.5. Adsorption isotherm

3.5.1. Langmuir isotherm

Langmuir isotherm is expressed by the following equation:

$$C_e/q_e = 1/(q_m \cdot K_L) + C_e/q_m \tag{6}$$

where K_L is the Langmuir adsorption constant (L/mg), C_e is the equilibrium As(V) concentration (mg/L) and q_m the adsorption capacity (mg/g).

Linear plot of C_e/q_e vs. C_e indicated that the As(V) adsorption on the HPA-Fe/C-B adsorbent followed the Langmuir isotherm (Fig. 11). The q_m and K_L constants were calculated from the regression line slopes and intercepts and are listed in Table 2.

The nature of the Langmuir isotherm can be described using the equilibrium constant or separation factor (R_L):

$$R_L = 1/(1 + K_L C_o) \tag{7}$$

where C_o is the initial As(V) concentration (mg/L).

The Langmuir isotherm is valid to homogeneous adsorption, where each adsorbate molecule is adsorbed onto the adsorbent surface with the same adsorption activation energy. The fitting result showed that the Langmuir isotherm yielded a good fit for the As(V) adsorption onto the HPA-Fe/C-B adsorbent, with the correlation coefficients (R^2) of 0.9675, 0.9660 and 0.9728 for the adsorption at 25°C, 35°C and 45°C, respectively (Fig. 11 and Table 2). The high R^2 values indicated the homogeneous character of the adsorbent surface. R_L values show the isotherm types to be irreversible ($R_L < 0$), linear ($R_L = 1$), favourable ($0 < R_L < 1$) or unfavourable ($R_L > 1$) [26]. The R_L values of 0.2856~0.3103 confirmed the favourable adsorption uptake of As(V).

3.5.2. Freundlich isotherm

The Freundlich isotherm as an empirical model is usable for multi-layer non-ideal adsorption that relates to hetero-
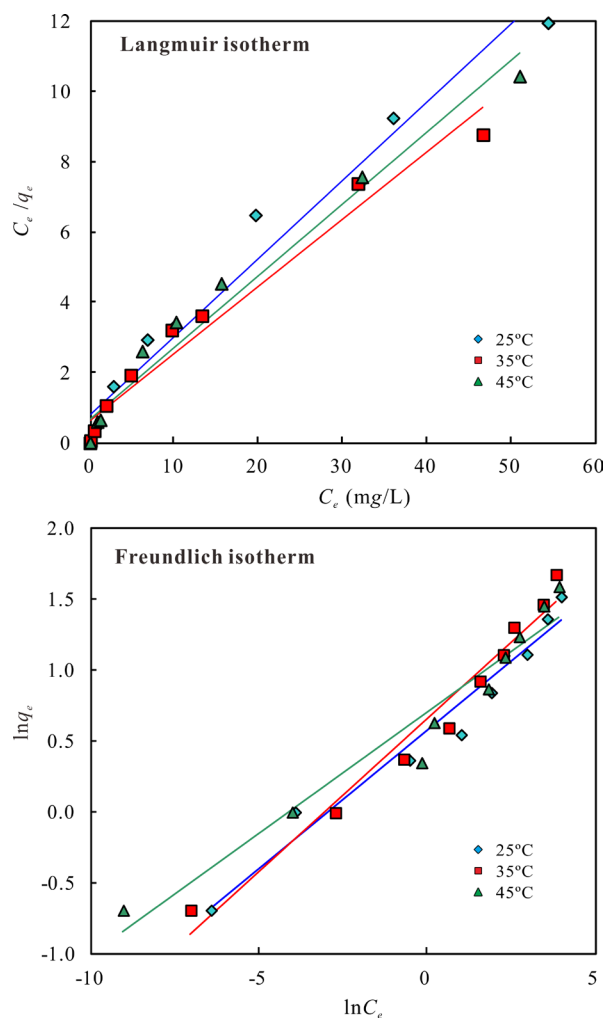
Fig. 11. Isotherm for the As(V) adsorption onto the HPA-Fe/C-B adsorbent (initial pH = 3; adsorbent dose 0.5 g/50 mL; adsorbent grain size <100 mesh)

geneous surface energy [24]. The Freundlich isotherm is expressed as:

$$\ln q_e = \ln K_F + 1/n \ln C_e \tag{8}$$

where K_F and $1/n$ are the Freundlich adsorption constant K_F (mg$^{1-1/n}$L$^{1/n}$g^{-1}) and the adsorption intensity, respectively.

The K_F and $1/n$ values were determined from the straight-line intercepts and slope of the plots (Fig. 11, Table 2). The Freundlich isotherm showed a good fit with the correlation coefficients (R^2) of 0.9615, 0.9682 and 0.9456 for the adsorption at 25°C, 35°C and 45°C, respectively. The $1/n$ values of 0.1711~0.2153, which were within 0~1, indicated a chemical adsorption [26].

3.6. Arsenate adsorption mechanisms

The arsenate adsorption is strongly dependent on the point of zero charge of adsorbents, at which the net charge of the adsorbent surface is neutral and the solution pH is defined as pH$_{PZC}$. When the pH$_{PZC}$ value is higher than the

solution pH, the acidic solution can provide more H^{+} ions than the adsorbent particle surface. As a result, the particle surface is positively charged, and it tends to attract anions and repel cations. On the contrary, when the pH_{PZC} value is lower than the solution pH, the particle surface is negatively charged, and it tends to attract cations and repel anions [44]. The change of the adsorption efficiency with the solution pH is related to the affinity of the HPA-Fe/C-B adsorbent with the arsenate species present. The pH_{PZC} values of the HPA-Fe/C-B adsorbent, Fe_3O_4, α-Fe_2O_3 and the bamboo charcoal were 3.1, 5.7, 5.2 and 2.3, respectively. In the acidic aqueous solution, the iron oxides surface is positively charged. The magnetite nanoparticle had a pH_{PZC} of 5.9 [45]. The magnetite particles showed a negative surface charge at pH 6.8~9.5, a point of zero charge at pH 6.8, and a positive surface charge at pH <6.8 [10]. The pH_{PZC} values were determined to be 6.7 for hematite and 6.5 for magnetite [46]. In the present work, the pH_{PZC} of the HPA-Fe/C-B adsorbent (3.1) was lower than that of magnetite and hematite. Above these pH_{PZC}, iron oxides exist in monomeric anionic forms, and thus show no affinity for arsenate anions. The HPA-Fe/C-B adsorbent can adsorb either positively or negatively charged ions through electrostatic attraction depending on solution pHs.

The amount of the positively charged sites on the adsorbent particle surface together with arsenate speciation determined the pH reliance of arsenate adsorption by magnetite and hematite. In the aqueous solution of pH 1~10, As(V) occurs mainly as H_3AsO_4, $H_2AsO_4^-$ and $HAsO_4^{2-}$, which can be strongly adsorbed onto the positively charged surface sites of iron oxides when the solution pH is lower than their pH_{PZC} (Fig. 12). Magnetite releases Fe^{2+} and various hydrolysis species ($Fe(OH)_3^-$, $Fe(OH)_2^0$ and $FeOH^+$) will form depending on the solution pH [28,47]. When pH < 5.6 (pK_{a1}), main functional groups on the solid surface are Fe^{2+} or $FeOH^+$, i.e., magnetite can attract negatively charged species. When pH > 5.6, the main functional hydroxyl groups on the solid surface are $Fe(OH)_3^-$ and $Fe(OH)_2^0$, the negatively charged adsorbent surface repelled negatively charged species [28,47].

The As(V) adsorption onto magnetite and hematite may involve three kinds of chemical reactions [47,48], i.e., forming of the mono-dentate inner sphere complexes on iron oxides through replacing of the singly coordinated surface hydroxyl groups by the arsenate species $HAsO_4^{2-}$ (9); protonation of the arsenate species adsorbed (10,11), and deprotonation and protonation of the singly coordinated surface hydroxyl (12,13). In the present work, the protonation reactions (10), (11) and (12) occurred when pH < 5.5~6.5 and the H^{+} consumption caused a pH increase. When pH > 5.5~6.5, the deprotonation reaction (15) occurred and the solution pH decreased (Fig. 12).

$$\equiv Fe-OH + HAsO_4^{2-} = \equiv Fe-AsO_4^{2-} + H_2O \tag{9}$$

$$\equiv Fe-AsO_4^{2-} + H^+ = \equiv Fe-AsO_4H^- \tag{10}$$

$$\equiv Fe-AsO_4H^- + H^+ = \equiv Fe-AsO_4H_2 \tag{11}$$

$$\equiv Fe-OH + H^+ = \equiv Fe-OH_2^+ \tag{12}$$

$$\equiv Fe-OH = \equiv Fe-O^- + H^+ \tag{13}$$
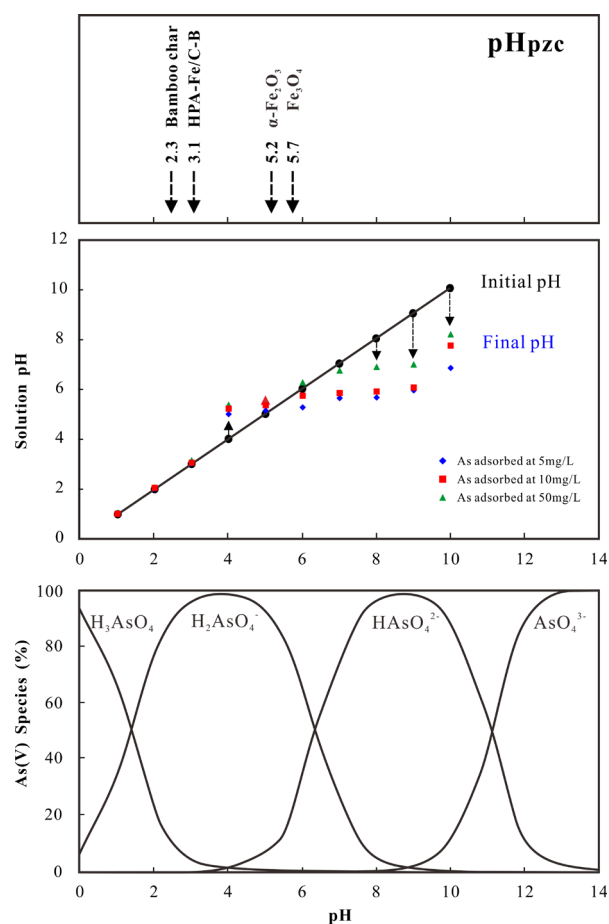
Fig. 12. Variation of the solution pH during the As(V) adsorption onto the HPA-Fe/C-B adsorbent.

4. Conclusions

The HPA-Fe/C-B adsorbent retained the hierarchical porous microstructure of bamboo bio-template with three kinds of pores (widths 50~75 µm, 1~30 µm and 0.0017~0.2891 µm) originating from vessels, fibres or parenchyma cells and pits on the walls of the vessels and parenchyma cells, respectively. The BET surface area of the HPA-Fe/C-B adsorbent was 198.1 m²/g.

The HPA-Fe/C-B adsorbent could effectively remove arsenate oxyanions from water. The As(V) adsorption onto the pulverized HPA-Fe/C-B adsorbent (<0.149 mm) at 25°C and pH 3 attained equilibrium after 20, 360 and 720 min for the initial As(V) concentrations of 5, 10 and 50 mg/L, respectively. For the adsorption onto the pulverized HPA-Fe/C-B adsorbent (<0.149 mm), with the increasing initial As(V) concentration from 5 to 100 mg/L, the amounts of As(V) adsorbed increased from 0.50 mg/g to 4.55 mg/g at 25°C, 0.50 mg/g to 5.33 mg/g at 35°C and 0.50 mg/g to 4.89 mg/g at 45°C. The removal percentages decreased from 99.97% to 45.58% at 25°C, 99.98% to 53.30% at 35°C and 100.00% to 48.94% at 45°C. For the adsorption onto the un-pulverized HPA-Fe/C-B adsorbent (>0.841 mm) with the initial As(V) concentrations of 5, 10 and 50 mg/L, the adsorption capacities were 0.45, 0.86 and 3.02 mg/g, the removal percentages were 90.75%, 86.66% and 61.24%, respectively.

The pseudo-second-order kinetic model fitted the experimental data very well with regression coefficients (R^2) >0.9989. The adsorption followed both Langmuir and Freundlich isotherms. The q_e values calculated from the models were also in consistent with the experimental data.

Acknowledgements

References

[1] WHO (World Health Organization), Arsenic, <http://www.who.int/mediacentre/factsheets/fs372/en/> (accessed: 30.09.2016).
[2] A.E. Smith, R.A. Lincoln, C. Paulu, T.L. Simones, K.L. Caldwell, R.L. Jones, L.C. Backer, Assessing arsenic exposure in households using bottled water or point-of-use treatment systems to mitigate well water contamination, Sci. Total Environ., 544 (2015) 701–710.
[3] G. Ungureanu, S. Santos, B. Rui, C. Botelho, Arsenic and antimony in water and wastewater: Overview of removal techniques with special reference to latest advances in adsorption, J. Environ. Manage., 151 (2015) 326–342.
[4] P.L. Smedley, D.G. Kinniburg, A review of the source, behaviour and distribution of arsenic in natural waters, Appl. Geochem., 17 (2002) 517–568.
[5] D. Mohan, C.U. Pittman, Arsenic removal from water/wastewater using adsorbents – A critical review, J. Hazard. Mater., 142 (2007) 1–53.
[6] J.A. Acosta, J.M. Arocena, A. Faz, Speciation of arsenic in bulk and rhizosphere soils from artisanal cooperative mines in Bolivia, Chemosphere, 138 (2015) 1014–1020.
[7] T. Mishra, D.K. Mahato, A comparative study on enhanced arsenic(V) and arsenic(III) removal by iron oxide and manganese oxide pillared clays from ground water, J. Environ. Chem. Eng., 4 (2016) 1224–1230.
[8] P. Sabbatini, F. Rossi, G. Thern, A. Marajofsky, M.M.F. de Cortalezzi, Iron oxide adsorbers for arsenic removal: a low cost treatment for rural areas and mobile applications, Desalination, 251 (2010) 184–192.
[9] S. Sinha, G. Amy, Y. Yoon, N. Her, Arsenic removal from water using various adsorbents: magnetic ion exchange resins, hydrous ion oxide particles, granular ferric hydroxide, activated alumina, sulfur modified iron, and iron oxide-coated microsand, Environ. Eng. Res., 16 (2011) 165–173.
[10] S. Yean, L. Cong, C.T. Yavuz, J.T. Mayo, W.W. Yu, A.T. Kan, V.L. Colvin, M.B. Tomson, Effect of magnetite particle size on adsorption and desorption of arsenite and arsenate, J. Mater. Res., 20 (2005) 3255–3264.
[11] S. Lata, S.R. Samadder, Removal of arsenic from water using nano adsorbents and challenges: A review, J. Environ. Manage., 166 (2016) 387–406.
[12] K. Ohe, T. Oshima, Y. Baba, Adsorption of arsenic using high surface area magnetites, Environ. Geochem. Hlth., 32 (2010) 283–286.
[13] M. Habuda-Stanić, B. Kalajdžić, M. Kuleš, N. Velić, Arsenite and arsenate adsorption by hydrousferric oxide/polymeric material, Desalination, 229 (2008) 1–9.
[14] H. Sieber, Biomimetic synthesis of ceramics and ceramic composites, Mat. Sci. Eng. A, 412 (2005) 43–47.
[15] Z.Q. Zhu, Y.N. Zhu, H. Qin, Y.H. Li, Y.P. Liang, H. Deng, H.L. Liu, Preparation and properties of porous composite of hematite/magnetite/carbon with eucalyptus wood biotemplate, Mater. Manuf. Process., 30 (2015) 285–291.
[16] M. Presas, J.Y. Pastor, J. LLorca, A.R. Arellano-López, J. Martínez-Fernández, R. Sepúlveda, Microstructure and fracture properties of biomorphic SiC, Int. J. Refract. Met. H., 24 (2006) 49–54.
[17] K. Lv, J. Li, X. Qing, W. Li, Q. Chen, Synthesis and photo-degradation application of WO_3/TiO_2 hollow spheres, J. Hazard. Mater., 189 (2011) 329–335.
[18] C. Su, R.W. Puls, Arsenate and arsenite sorption on magnetite: relations to groundwater arsenic treatment using zerovalent iron and natural attenuation, Water Air Soil Pollut., 193 (2008) 65–78.
[19] H.J. Shipley, S. Yean, A.T. Kan, M.B. Tomson, Adsorption of arsenic to magnetite nanoparticles: effect of particle concentration, pH, ionic strength, and temperature, Environ. Toxicol. Chem., 28 (2009) 509–515.
[20] S.R. Chowdhury, E.K. Yanful, Arsenic and chromium removal by mixed magnetite-maghemite nanoparticles and the effect of phosphate on removal, J. Environ. Manage., 91 (2010) 2238–2247.
[21] H. Wu, G. Wu, L. Wang, Peculiar porous α-Fe_2O_3, γ-Fe_2O_3 and Fe_3O_4 nanospheres: Facile synthesis and electromagnetic properties, Powder Technol., 269 (2015) 443–451.
[22] H. Wu, L. Wang, H. Wu, Q. Lian, Synthesis and significantly enhanced microwave absorption properties of hematite dendrites/polyaniline nanocomposites, Appl. Phys. A, 115 (2014) 1299–1307.
[23] H. Wu, L. Wang, H. Wu, Synthesis, characterization and microwave absorption properties of dendrite-like Fe_3O_4, embedded within amorphous sugar carbon matrix, Appl. Surf. Sci., 290 (2014) 388–397.
[24] H. Guo, D. Stüben, Z. Berner, Removal of arsenic from aqueous solution by natural siderite and hematite, Appl. Geochem., 22 (2007) 1039–1051.
[25] M. Doğan, Y. Özdemir, M. Alkan, Adsorption kinetics and mechanism of cationic methyl methylene blue dyes onto sepiolite, Dyes Pigments, 75 (2007) 701–713.
[26] G. Crini, Kinetic, equilibrium studies on the removal of cationic dyes from aqueous solution by adsorption onto a cyclodextrin polymer, Dyes Pigments, 77 (2008) 415–426.
[27] D.B. Singh, G. Prasad, D.C. Rupainwar, Adsorption technique for the treatment of As(V)-rich effluents, Colloids Surfaces A, 111 (1996) 49–56.
[28] R.M. Cornell, U. Schwertmann, The iron oxides: structure, properties, reactions, occurrences, and uses, second ed., Wiley-VCH, Weinheim, 2003.
[29] J. Giménez, M. Martínez, J. de Pablo, M. Rovira, L. Duro, Arsenic adsorption onto natural hematite, magnetite, and goethite, J. Hazard. Mater., 141 (2007) 575–580.
[30] G.J. Parsons, L.M. Lpoez, R.J. Peralta-Videa, L.J. Gardea-Torresdey, Determination of arsenic (III) and arsenic(V) binding to microwave assisted hydrothermal synthetically prepared Fe_3O_4, Mn_3O_4, and $MnFe_2O_4$ nanoadsorbents, Microchem. J., 91 (2009) 100–106.
[31] Y. Mamindy-Pajany, C. Hurel, N. Marmier, M. Roméo, Arsenic(V) adsorption from aqueous solution onto goethite, hematite, magnetite and zero-valent iron: Effects of pH, concentration and reversibility, Desalination, 281 (2011) 93–99.
[32] S. Aredes, B. Klein, M. Pawlik, The removal of arsenic from water using natural iron oxide minerals, J. Clean. Prod., 29–30 (2012) 208–213.
[33] S. Luther, N. Borgfeld, J. Kim, J.G. Parsons, Removal of arsenic from aqueous solution: a study of the effects of pH and interfering ions using iron oxide nanomaterials, Microchem. J., 101 (2012) 30–36.
[34] P. Xu, G.M. Zeng, D.L. Huang, C.L. Feng, S. Hu, M.H. Zhao, C. Lai, Z. Wei, C. Huang, G.X. Xie, Z.F. Liu, Use of iron oxide nanomaterials in wastewater treatment: a review, Sci. Total Environ., 424 (2012) 1–10.

[35] X. Hu, Z. Ding, A.R. Zimmerman, S. Wang, B. Gao, Batch and column sorption of arsenic onto iron-impregnated biochar synthesized through hydrolysis, Water Res., 68 (2015) 206–216.

[36] T. Türk, İ. Alp, Arsenic removal from aqueous solutions with Fe-hydrotalcite supported magnetite nanoparticle, J. Ind. Eng. Chem., 20 (2014) 732–738.

[37] A.V. Vitela-Rodriguez, J.R. Rangel-Mendez, Arsenic removal by modified activated carbons with iron hydro (oxide) nanoparticles, J. Environ. Manage., 114 (2013) 225–231.

[38] A.I. Okoye, P.M. Ejikeme, O.D. Onukwuli, Lead removal from wastewater using fluted pumpkin seed shell activated carbon: adsorption modeling and kinetics, Inter. J. Environ. Sci. Technol., 7 (2010) 793–800.

[39] Y.S. Ho, G. McKay, Pseudo-second order model for sorption processes, Process Biochem., 34 (1999) 451–465.

[40] D.L. Sparks, Kinetics of soil chemical processes, New York: Academic, 1989.

[41] G. Mckay, V.J.P. Poots, Kinetics and diffusion process in colour removal from effluent using wood as an adsorbent, J. Chem. Technol. Biot., 30 (1980) 279–292.

[42] X.Y. Yang, B. Al-Duri, Kinetic modeling of liquid-phase adsorption of reactive dyes on activated carbon, J. Colloid Interf. Sci., 287 (2005) 25–34.

[43] S. Kong, Y. Wang, H. Zhan, S. Yuan, M. Yu, M. Liu, Adsorption/oxidation of arsenic in groundwater by nanoscale Fe-Mn binary oxides loaded on zeolite, Water Environ. Res., 86 (2014) 147–155.

[44] G. Muñiz, V. Fierro, A. Celzard, G. Furdin, G. Gonzalez-Sánchez, M.L. Ballinas, Synthesis, characterization and performance in arsenic removal of iron-doped activated carbons prepared by impregnation with Fe(III) and Fe(II), J. Hazard. Mater., 165 (2009) 893–902.

[45] C.H. Weng, Y.T. Lin, C.L. Yeh, Y.C. Sharma, Magnetic Fe_3O_4 nanoparticles for adsorptive removal of acid dye (new coccine) from aqueous solutions, Water Sci. Technol., 62 (2010) 844–851.

[46] D.A. Sverjensky, Zero-point-of-charge prediction from crystal chemistry and salvation theory, Geochim. Cosmochim. Ac., 58 (1994) 3123–3129.

[47] Y. Zhu, Z. Zhu, Y. Chen, F. Yang, H. Qin, L. Xie, Kinetics and thermodynamics of sorption for As(V) on the porous biomorph-genetic composite of α-Fe_2O_3/Fe_3O_4/C with eucalyptus wood hierarchical microstructure, Water Air Soil Pollut., 224 (2013) Article Number 1589.

[48] X. Huang, Intersection of isotherms for phosphate adsorption on hematite, J. Colloid Interf. Sci., 271 (2004) 296–307.